5278 *Biochemistry* **2010,** *49,* 5278–5289
DOI: 10.1021/bi100111c

BIOCHEMISTRY
including biophysical chemistry & molecular biology
Article

Metamorphic Response of the CLIC1 Chloride Intracellular Ion Channel Protein upon Membrane Interaction[†]

Sophia C. Goodchild,[‡] Michael W. Howell,[‡] Dene R. Littler,[§,#] Ramya A. Mandyam,[‡,▽] Kenneth L. Sale,[∥] Michele Mazzanti,[⊥] Samuel N. Breit,[@] Paul M. G. Curmi,[§,@] and Louise J. Brown*[,‡]

[‡]*Department of Chemistry and Biomolecular Sciences, Macquarie University, Sydney, New South Wales 2109, Australia,* [§]*School of Physics, University of New South Wales, Sydney, New South Wales 2052, Australia,* [∥]*Biosystems R&D Department, Sandia National Laboratories, Livermore, California 94551,* [⊥]*Dipartimento di Scienze Biomolecolari e Biotecnologie, Universita' degli Studi di Milano, Via Celoria 26, 20133 Milano, Italy, and* [@]*St. Vincent's Centre for Applied Medical Research, St. Vincent's Hospital, and University of New South Wales, Sydney, New South Wales 2010, Australia* [#]*Current address: The Netherlands Cancer Institute, Division of Molecular Carcinogenesis, Plesmaanlaan 121, 1066 CX Amsterdam, The Netherlands.*
[▽]*Current address: Institute for Biomolecular Sciences, Division of Molecular Cell Biology, QBP, University of Queensland, Brisbane, QLD 4072, Australia.*

Received January 25, 2010; Revised Manuscript Received April 29, 2010

ABSTRACT: A striking feature of the CLIC (chloride intracellular channel) protein family is the ability of its members to convert between a soluble state and an integral membrane channel form. Direct evidence of the structural transition required for the CLIC protein to autonomously insert into the membrane is lacking, largely because of the challenge of probing the conformation of the membrane-bound protein. However, insights into the CLIC transmembrane form can be gained by biophysical methods such as fluorescence resonance energy transfer (FRET) spectroscopy. This approach was used to measure distances from tryptophan 35, located within the CLIC1 putative N-domain transmembrane region, to three native cysteine residues within the C-terminal domain. These distances were computed both in aqueous solution and upon the addition of membrane vesicles. The FRET distances were used as constraints for modeling of a structure for the CLIC1 integral membrane form. The data are suggestive of a large conformational unfolding occurring between the N- and C-domains of CLIC1 upon interaction with the membrane. Consistent with previous findings, the N-terminal domain of CLIC1 is likely to insert into the lipid bilayer, while the C-domain remains in solution on the extravesicular side of the membrane.

Traditionally, it has been thought that proteins adopt a well-defined tertiary structure, with at most small conformational changes accompanying function. However, it is becoming increasingly apparent that some proteins can shift between two or more stable conformations, a property termed "metamorphic" (*1*). This metamorphic property is a prominent feature of the unique CLIC[1] (chloride intracellular channel) protein family. In stark contrast to members of the traditional ion channel families, the CLICs are expressed as soluble proteins, with a conserved glutathione *S*-transferase (GST) superfamily-like fold that lacks both a leader sequence for membrane targeting and a clearly defined hydrophobic transmembrane domain. However, integration of recombinant CLIC protein into artificial, synthetic lipid bilayers to display ion channel activity has been demonstrated for CLIC members (*2*−*10*). In addition, recent evidence has suggested other canonical GST proteins may also possess membrane-transversing properties (*11*). However, both the biochemical and structural bases of the novel, automomous mechanism of CLIC membrane insertion remain unclear.

Since identification of the first CLIC protein and its mRNA transcript in humans in 1997 (*12*), much has been learned about this highly conserved six-member protein family (CLIC1−6). CLIC homologues have also been identified in invertebrates such as nematodes (*13*) and insects (*14*) and, more recently, in plants (*15*). Each CLIC homologue possesses a highly conserved C-terminal "CLIC module" of ∼240 amino acids, with some members also possessing additional, unrelated N-terminal domains. Overall, the high degree of sequence similarity shared among members of the CLIC family and preservation of a defined set of CLIC orthologues throughout vertebrate evolution intuitively implies evidence of their physiological importance (*16*). Although a clear elucidation of the molecular, cellular, and physiological function of the CLIC proteins, including their ion conducting role, is still in its infancy, members of the CLIC family have also been implicated in many fundamental processes, including cellular division (*17*, *18*), apoptosis and response to DNA damage (*19*−*21*), bone resorption (*22*), and tubulogenesis (*13*, *23*−*26*), to name a few.

Because of the difficulty in obtaining direct structural data of the transmembrane CLIC state, structural characterization of the CLICs has so far been limited to the soluble form. The soluble monomeric GST-like CLIC fold consists of two domains: a

[†]Supported by an Australian Research Council (ARC) grant and an ARC APD fellowship to L.J.B.

*To whom correspondence should be addressed: Department of Chemistry and Biomolecular Sciences, Macquarie University, Sydney, New South Wales 2109, Australia. Telephone: +61 2 9850 8294. Fax: +61 2 9850 8313. E-mail: Louise.Brown@mq.edu.au.

[1]Abbreviations: CLIC, chloride intracellular channel; FRET, fluorescence resonance energy transfer; EPR, electron paramagnetic resonance; PTM, putative transmembrane region encompassing Cys24−Val46 in CLIC1; WT, wild type; IAEDANS, 5-(iodoacetamidoethyl)aminonaphthalene-1-sulfonic acid; BDMC, 4-bromomethyl-6,7-dimethoxycoumarin; HNB, 2-hydroxy-5-nitrobenzene; MTSSL, 3-methylthiosulfonyl-1-oxyl-2,2,5,5-tetramethyl-Δ3-pyrroline.

 Published on Web 05/27/2010

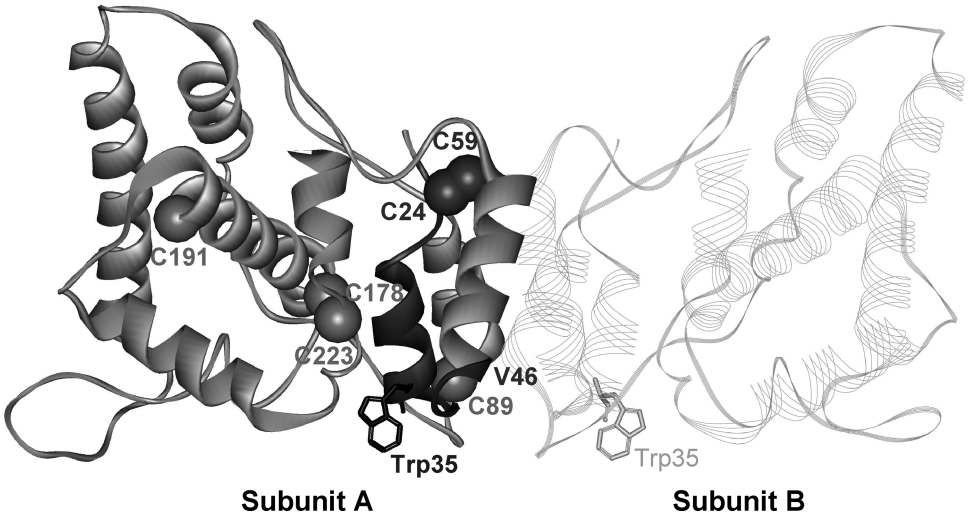

FIGURE 1: Location of single tryptophan residue (Trp35) and native CLIC1 cysteine residues (Cys24, Cys59, Cys89, Cys178, Cys191, and Cys223) mapped onto one subunit of the oxidized CLIC1 dimer (*6*). An intramolecular disulfide bond is formed between Cys24 and Cys59 upon oxidation. The four remaining native cysteines (Cys89, Cys178, Cys191, and Cys223) were selectively modified individually with fluorescent or EPR spin-labels. FRET distances were measured between Trp35 and the four labeled cysteines in solution and in the presence of lipid. The PTM region is from Cys24 to Val46 (black).

thioredoxin-like N-domain containing a glutathione binding site and an all-α-helical C-domain. The presence of the conserved glutathione binding site in the CLIC soluble monomer form led to the suggestion that chloride ion channel activity of the CLICs may be under the control of redox-active signaling molecules in vivo (*2*). Indeed, upon oxidation, the N-domain of monomeric CLIC1 was shown to undergo a major structural rearrangement, resulting in the exposure of a large hydrophobic surface that forms the interface between the two subunits of a soluble noncovalent dimer form (Figure 1). An intrasubunit disulfide bond is also formed between residues Cys24 and Cys59. The oxidized CLIC1 dimer maintains the ability to form chloride ion channels in artificial bilayers, while a reducing environment is unfavorable for the formation of functional ion channels (*6*). The suggestion was made that, in the presence of the lipid bilayer and under oxidative conditions, the hydrophobic dimer interface may dock to the membrane and, in doing so, form a precursor to the CLIC1 integral membrane form (*6*). The Cys24 residue, which is conserved among all human CLICs, may have a role in this process. However, the physiological relevance of the CLIC1 oxidized dimer state remains unclear, particularly since this state has been observed only for CLIC1.

In the absence of any significant structural insights into the transmembrane CLIC form, the ability of CLIC1 to undergo oxidation-induced metamorphosis in the absence of the bilayer reinforces the notion that CLIC proteins are capable of undergoing large-scale conformational rearrangement. Although current models for the structural transition between the soluble and transmembrane states of the CLICs remain highly speculative (*2*, *6*, *7*, *10*, *27*, *28*), current evidence suggests the CLIC proteins adopt a transmembrane form in which the N- and C-termini are on opposite sides of the bilayer (*29*). Proteolytic digestion studies have shown that residues ~20−50 of the "CLIC module" are unexposed in the integral membrane form (*30*), while fluorescence studies suggest residue Trp35 becomes buried in the bilayer upon membrane insertion (*10*). This model therefore accepts the existence of a single putative transmembrane region (PTM) encompassing residues Cys24−Val46 of the N-domain. This roughly corresponds to helix α1 and strand β2 of the CLIC1 monomer, which encompasses the glutathione binding site, or helices α1 and α2 of the oxidized CLIC1 dimer. For the CLICs to transit between soluble and integral membrane forms, the mechanism of membrane insertion must involve a large-scale conformational change within the CLIC module to confer favorable interactions with the membrane. This likely involves an unfolding or separation of the CLIC N-terminal domain away from its C-domain which allows the N-terminal PTM to traverse the membrane in an extended conformation. However, direct structural experimental support for such a dramatic conformational change upon interaction with the membrane is lacking.

In this study, we have sought to obtain evidence of the structural rearrangement of CLIC1 in the presence of a lipid bilayer. Fluorescence resonance energy transfer (FRET) and electron paramagnetic resonance (EPR) were used to monitor changes in distances and mobility, respectively, of the CLIC1 structure during the transition between the soluble and integral membrane forms. We employed a novel labeling strategy, utilizing the oxidative properties of CLIC1, to selectively target three of CLIC1's six native cysteine residues (Cys89, Cys178, and Cys223) with fluorescent or EPR labels (Figure 1). From membrane-induced changes in the FRET distances between the PTM (Trp35) and each of the three labeled native cysteines, a model of the CLIC membrane structure was developed using rigid body motion. The most notable feature of our model is the radical movement of the CLIC1 C-domain lobe away from its N-domain upon interaction with the membrane.

MATERIALS AND METHODS

CLIC1 Constructs, Expression, and Purification. Cysteine to serine mutations were generated on the CLIC1 protein sequence (GenBank accession number CAG46868) using the QuikChange site-directed mutagenesis kit (Stratagene). A CLIC1 construct retaining Cys24 and Cys59 ($CLIC1_{24/59}$) and four "single-cysteine" constructs with only one of the four remaining native cysteines at positions 89, 178, 191, or 223 were created. The following nomenclature is used to describe these constructs: $CLIC1_{24/59}(+Cys89)$, $CLIC1_{24/59}(+Cys178)$, $CLIC1_{24/59}(+Cys191)$,

or CLIC1$_{24/59}$(+*Cys223*), respectively. For example, mutant CLIC1$_{24/59}$(+*Cys223*) has Cys24 and Cys59 unmodified for dimer formation and also possesses Cys223 for subsequent labeling (Figure 1). All constructs were confirmed by DNA sequencing.

Recombinant glutathione *S*-transferase (GST) fusion proteins (GST−CLIC1 wild type, −CLIC1$_{24/59}$, and −CLIC1 cysteine mutants, as described above) were expressed in *Escherichia coli* BL21(DE3) cells using the pGEX-4T-1 vector (Amersham Biosciences) and purified as previously described (*6*). Briefly, cells were grown in 2× YT medium, and expression of the soluble GST−CLIC1 fusion constructs were induced at 20 °C by the addition of 1 mM IPTG at midlog growth phase. Cells were harvested after 16 h, and the fusion protein was isolated from the soluble fraction by binding to glutathione *S*-Sepharose 4B resin in the presence of 0.3 mM dithiothreitol (DTT) (Amersham Biosciences). The CLIC1 constructs were cleaved from the GST tag overnight using 30 NIH units of bovine plasma thrombin (Sigma-Aldrich) per liter of *E. coli* culture. Reduced CLIC1 monomer was also obtained in the presence of 1 mM DTT and further purified using a Superdex 75 prep grade high-performance size exclusion chromatography (SEC) column (GE Healthcare) equilibrated in 100 mM KCl, 1 mM DTT, 1 mM NaN_3, and 20 mM HEPES (pH 7.5).

Oxidation and Isolation of the CLIC1 Dimer. To protect Cys24 and Cys59 from undesired modification with the extrinsic thiol reactive labels, the oxidized dimer form of the CLIC1 constructs was obtained by treatment with hydrogen peroxide (H_2O_2), as previously described (*6*). H_2O_2 was added to 6 mL of purified protein, between 2 and 8 mg/mL in phosphate-buffered saline (PBS) (pH 7.3), to a final concentration of 2 mM. The reaction was allowed to continue for 2 h at 4 °C before injection of the oxidized protein onto a Superdex 75 prep grade SEC column (GE Healthcare) pre-equilibrated in 100 mM KCl, 1 mM NaN_3, and 20 mM HEPES (pH 7.5). The column was calibrated with the standard proteins ribonuclease A (13.7 kDa), chymotripsinogen A (25 kDa), ovalbumin (43 kDa), and aldolase (158 kDa), and the column void volume was determined from the elution of blue dextran (2×10^6 kDa).

Fluorescent Labeling of Cys89, Cys178, Cys223, and Trp35. The purified oxidized CLIC1 dimer constructs containing single cysteines available for labeling (Cys89, Cys178, and Cys223) were specifically modified with IAEDANS [5-(iodoacetamidoethyl)aminonaphthalene-1-sulfonic acid] as the FRET acceptor probe in the presence of intrinsic tryptophan fluorescence. Cys223 was also modified with BDMC (4-bromomethyl-6,7-dimethoxycoumarin) as the FRET donor probe for the BDMC−HNB FRET pair. Labeling was performed in the absence of DTT to maintain the Cys24−Cys59 intramolecular disulfide bond and allow for specific labeling of the remaining free single cysteine. Specifically, the CLIC1-oxidized dimer eluted via SEC was concentrated to 1−2 mg/mL using an Amicon Ultra-15 centrifugal filter device (Millipore) and buffer exchanged into assay buffer [150 mM NaCl and 50 mM Tris-HCl (pH 8.0)]. A 5-fold molar excess of IAEDANS or BDMC was added, and the sample was incubated at 4 °C for 4 h, before the addition of a further 2-fold molar excess of label. The reaction was allowed to continue at 4 °C for 16 h. Unreacted label was removed by extensive dialysis against assay buffer. Where possible, all steps involving IAEDANS and BDMC were performed in the dark to prevent photobleaching.

For the CLIC1$_{24/59}$(+*Cys223*) construct, the PTM Trp35 was also modified with the fluorescent acceptor label HNB (2-hydroxy-5-nitrobenzene) for measurements of the distance from BDMC-modified Cys223. Specific labeling of Trp35 with HNB was achieved by addition of a 10-fold molar excess of dimethyl (2-hydroxy-5-nitrobenzyl)sulfonium bromide (Sigma) to the protein sample in 50 mM sodium phosphate (pH 6.5) for 20 min at 4 °C. The reaction was terminated when the mixture was passed through a HiTrap desalting column (GE Healthcare Life Sciences) equilibrated in assay buffer followed by dialysis against the same buffer to ensure all unreacted label was removed.

Labeling ratios were determined spectrophotometrically using a molar absorption coefficient ε of 6.3×10^3 M^{-1} cm^{-1} at 337 nm for IAEDANS (*31*), 12.9×10^3 M^{-1} cm^{-1} at 354 nm for BDMC (*32*), and 18.0×10^3 M^{-1} cm^{-1} at 410 nm and pH >12 for HNB (*33*). Protein concentrations were determined spectrophotometrically, using an absorbance coefficient of 16.2×10^3 M^{-1} cm^{-1} at 280 nm, or by a BCA assay (Pierce) using bovine serum albumin (BSA) protein standards.

Preparation of Liposomes. Soybean phosphatidylcholine (Sigma catalog no. P-5638) and cholesterol (Sigma catalog no. C-8667) were dissolved in chloroform and mixed at a ratio of 10:1 (w/w). Solvent was evaporated under a N_2 stream to form a thin lipid film over the bottom of a glass tube, and the mixture was further dried under vacuum for 3 h. Lipids were rehydrated at 40 mg/mL in assay buffer [150 mM NaCl and 50 mM Tris-HCl (pH 8.0)] for 30 min on ice, while being vortexed intermittently in the presence of glass beads. The resultant lipid suspension was extruded through 100 or 400 nm polycarbonate filters using a mini-extruder LiposoFast Basic apparatus (Avestin) to produce unilamellar liposome vesicles. The integrity of lipids was ensured by their storage on ice and the use of the vesicles within 2 days of rehydration.

Fluorescence Measurements. Steady-state fluorescence intensity spectra were recorded at room temperature (22 °C) using a Perkin-Elmer LS50B fluorimeter operating in ratio mode and FL WinLab version 3.0. For the Trp−IAEDANS donor−acceptor pair, samples were excited at a tryptophan excitation wavelength of 290 nm, and emission was monitored from 300 to 550 nm. For the BDMC−HNB donor−acceptor pair, samples were excited at a BDMC excitation wavelength of 350 nm, and emission was monitored from 360 to 600 nm. All data were collected using 6 μM protein samples in assay buffer using a spectral bandwidth of 4−6 nm.

For the CLIC1 FRET distance between an IAEDANS-labeled cysteine residue and Trp35, spectra were first collected from a sample of unlabeled CLIC1 (Trp35 donor only, D) and a labeled sample with a single IAEDANS fluorophore acceptor at either position Cys89, Cys178, or Cys223 (DA). For the Cys223−Trp35 distance using the BDMC−HNB donor−acceptor pair, the donor spectrum (D) of Trp35-BDMC-labeled CLIC1$_{24/59}$(+*Cys223*) was first recorded followed by the DA spectrum of BDMC/HNB-labeled CLIC1$_{24/59}$(+*Cys223*); 100 nm liposomes were added directly to both the D and DA samples to a concentration of 1.4 mM, and spectra were recorded at 0 h (within ~2 min to allow for mixing), 4 h, 8 h, and 24 h. Spectra were corrected for background fluorescence by subtraction of scatter from a 1.4 mM liposome solution. Inner filter and self-absorption effects were minimized by ensuring that the absorbance of all samples at the excitation wavelength was kept below 0.05.

Fluorescence Resonance Energy Transfer Analysis. Fluorescence resonance energy transfer efficiency (*E*) was

calculated from the D emission intensity according the following relationship (*34*)

$$E = 1 - \frac{F_{DA} - F_D(1 - f_A)}{F_D f_A} \quad (1)$$

where E is the efficiency of energy transfer calculated, F_{DA} is the fluorescence intensity maximum of the donor in the presence of the acceptor, F_D is the donor fluorescence intensity maximum in the absence of acceptor, and f_A is the fractional labeling of the acceptor site The donor−acceptor distance (R) was then obtained from the measured transfer efficiencies using the Förster equation

$$R = (E^{-1} - 1)^{1/6} R_0 \quad (2)$$

where R_0 is the Förster critical distance at which $E = 50\%$. The value of R_0, depending on the donor−acceptor pair, is given by

$$R_0 = (9.78 \times 10^3)[\kappa^2 n^{-4} Q_D J(\lambda)]^{1/6} \text{ (Å)} \quad (3)$$

where κ_2 is the dipole interaction orientation factor (assumed to be $^2/_3$), n is the refractive index of the medium (1.33), Q_D is the quantum yield of the donor in the absence of the acceptor, and $J(\lambda)$ is the overlap integral, calculated from

$$J(\lambda) = \frac{\int_0^\infty F_D(\lambda)\varepsilon_A(\lambda)\lambda^4 \, d\lambda}{\int_0^\infty F_D(\lambda) \, d\lambda} \quad (4)$$

where $F_D(\lambda)$ is the fluorescence intensity of the donor at wavelength λ and $\varepsilon_A(\lambda)$ is the molar absorbance of the acceptor at wavelength λ. The overlap integrals of the CLIC1 Trp35 donor and IAEDANS acceptor and BDMC and HNB were calculated by numerical integration. The quantum yield of CLIC1 Trp35 was determined using anthracene as a reference [quantum yield of 0.27 in ethanol at 25 °C (*35*)].

Electron Paramagnetic Resonance Spectroscopy. Cys89, Cys178, and Cys223 of the CLIC1$_{24/59}$(+*Cys89*), CLIC1$_{24/59}$(+*Cys178*), and CLIC1$_{24/59}$(+*Cys223*) constructs, respectively, were modified with the nitroxide spin-label MTSSL [3-methylthiosulfonyl-1-oxyl-2,2,5,5-tetramethyl-Δ3-pyrroline (Toronto Research Chemicals)] using the same method as described for fluorescent labeling. EPR spectroscopy was performed on a Bruker 9.5 GHz EMX X-band spectrometer using a standard rectangular TE102 cavity at room temperature. First-derivative EPR absorption spectra were recorded with a microwave power of 5.0 mW, a modulation amplitude of 1.0 G, a modulation frequency of 100 kHz, and a sweep width of 120 G. EPR spectra were averaged and analyzed using spectral analysis software written in LabView (P. Fajer, Florida State University, Tallahassee, FL). Spectra of the spin-labeled CLIC1 dimer were collected in assay buffer and upon addition of 400 nm large unilamellar phospholipid vesicle liposomes at final concentrations of ~50 μM CLIC1 and 26 mM lipid. The membrane-bound EPR signal was obtained by EPR spectral subtraction.

Circular Dichroism. A Jasco J-810 CD spectropolarimeter was used to record far-UV CD spectra (190−260 nm) of CLIC1 WT oxidized dimer and CLIC1$_{24/59}$ oxidized dimer in CD buffer [50 mM NaF and 10 mM $NaPO_4$ (pH 6.5)] at 0.1 mg/mL. Spectra were recorded using a 0.1 mm path length quartz cuvette at 21 °C. A total of eight scans were collected for analysis using the following spectral parameters: scan rate of 100 nm/min, resolution of 0.1 nm, bandwidth of 1 nm, sensitivity of 10 mdeg, and response time of 4 s. Ellipticity values are reported as the mean residue molar ellipticity ([θ], degrees square centimeter per decimole) using the equation

$$[\theta] = \frac{\text{CD(mdeg)} \times \text{MRW}}{10lc} \quad (5)$$

where CD(mdeg) is the baseline-corrected ellipticity in millidegrees, MRW is the mean residue mass (120 Da for CLIC1), l is the optical path length in centimeters, and c is the concentration in milligrams per milliliter.

Free Sulfhydryl Content. An Ellman's reagent assay was used to quantitate free sulfhydryl groups in the CLIC1 WT monomer and dimer and CLIC1$_{24/59}$ samples, both in the soluble state and upon addition of lipids. Samples were prepared by mixing 100 μL of 10 mM Ellman's reagent [DTNB, 5,5′-dithiobis(2-nitrobenzoic acid)] with 2.6 mL of 7.5 μM CLIC1 in 1 mM EDTA and 100 mM sodium phosphate (pH 8.0). For samples containing lipid, 100 nm extruded liposomes were added to a final concentration of 0.75 mM. Samples were incubated at room temperature for 15 min before the absorbance was measured at 412 nm. The free sulfhydryl content for each CLIC1 sample was determined using cysteine hydrochloride monohydrate standards, and thus, the number of free cysteine equivalents per CLIC1 molecule was obtained.

Modeling of CLIC1 from FRET Distance Constraints. The structure of the soluble oxidized half-dimer of CLIC1 (Protein Data Bank entry 1RK4) was used as the starting structure with which to model conformational rearrangement consistent with the changes in FRET distances observed upon interaction with the membrane. The intramolecular disulfide bond between Cys24 and Cys59 was reduced, and residues 22−46 of the PTM were modeled as an extended α-helix, as previously proposed (*27*, *28*), to allow the CLIC1 N-domain to span the bilayer. Rigid body minimization was performed in which residues 59−78 and residues 91−110 were treated as flexible "hinge" regions, and residues 22−58, 79−90, and 111−234 were treated as rigid bodies. Energy minimization was performed in a series of stages in which energy terms were included in such a way, first, to force satisfaction of FRET membrane distance constraints and then to remove any resulting bad contacts. Stage one consisted of 1000 steps of the limited-memory Broyden−Fretcher−Goldfarb−Shanno (L-BFGS) minimization of the crystal structure of the soluble protein. In stage two, we included the FRET distances as NOE constraints in CNX. Distance constraints were applied between the CH2 atom on the Trp35 ring and the S group of the cysteine. For each distance, an error of ±4 Å was allowed to account for the fact that we cannot explicitly model the probe attached to the cysteine residue. The constrained structure was energy minimized using 1000 steps of L-BFGS minimization in which only the bond and NOE energy terms were included (*36*, *37*). This was done to allow the protein to freely move through space without steric impedance. In stage three, all energy terms, including the NOE term, were turned on and the structure satisfying the set of FRET distances was minimized using 1000 steps of L-BFGS minimization.

RESULTS

Formation of the Redox-Induced CLIC1 Dimerization Construct. An unusual characteristic of CLIC1 is that it possesses the ability to form a noncovalent soluble dimer under oxidative conditions (*6*). Purified recombinant CLIC1 was oxidized prior to injection onto a SEC column to isolate the CLIC1 dimer species (Figure 2a). Wild-type (WT) CLIC1, under reducing conditions (1 mM DTT), eluted as a monomeric species,

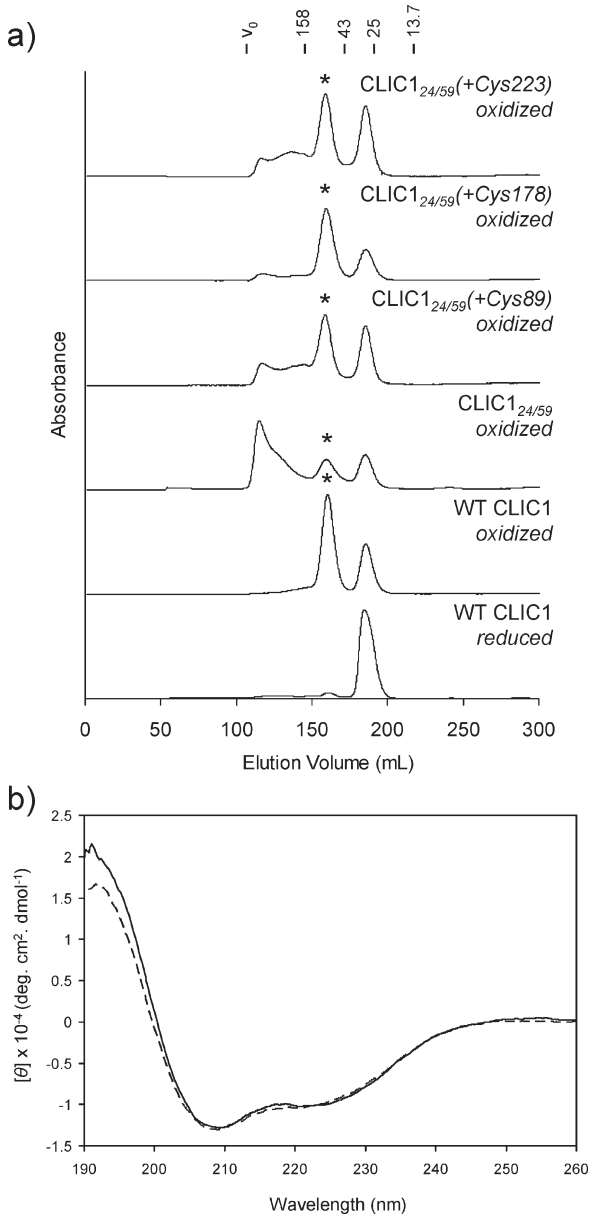

FIGURE 2: Formation of the oxidized CLIC1 dimer constructs. (a) Superdex G75 size exclusion purification of oxidized CLIC1 WT, CLIC1$_{24/59}$, and single-cysteine mutants. The ordinate shows the absorbance at 280 nm, with a flow rate of 0.8 mL/min. Oxidized dimer (*) is eluted at ~165 mL, followed by the monomeric CLIC1 form at ~190 mL. A high-molecular mass species (at ~110−140 mL) is evident and unresolved. From bottom to top: WT CLIC1 under reducing conditions (2 mM DTT), oxidized WT CLIC1 (2 mM H_2O_2 for 2 h at 4 °C), oxidized CLIC1$_{24/59}$, oxidized CLIC1$_{24/59}$(+*Cys89*), oxidized CLIC1$_{24/59}$(+*Cys178*), and oxidized CLIC1$_{24/59}$(+*Cys223*). (b) Circular dichroism of oxidized dimer CLIC1$_{24/59}$ (···) compared to WT CLIC1 (—). Spectra were recorded in 50 mM NaF and 10 mM $NaPO_4$ (pH 6.5) at 21 °C.

while the addition of 2 mM H_2O_2 for 2 h at 4 °C resulted in the formation of an oxidized dimer species, comprising up to approximately two-thirds of the total WT CLIC1 protein. Formation of the dimer species was also observed for the CLIC1$_{24/59}$ mutant under the same optimized conditions, demonstrating that the disulfide bond formed between Cys24 and Cys59 upon oxidation was preserved despite mutagenesis of the four remaining native cysteine residues to serine. However, the proportion of CLIC1$_{24/59}$ forming dimers was slightly lower than the proportion of the WT. Noticeably, a large proportion of CLIC1$_{24/59}$ also eluted as a high-molecular mass species. This was also observed during H_2O_2 treatment of the single-cysteine mutants, although to a lesser extent. The three single mutants [CLIC1$_{24/59}$(+*Cys89*), CLIC1$_{24/59}$(+*Cys178*), and CLIC1$_{24/59}$(+*Cys223*)] all formed significant quantities of the oxidized dimer, representing between one-half and two-thirds of the total CLIC1 yield. The exception was the CLIC1$_{24/59}$(+*Cys191*) mutant (not shown) where insufficient dimer yields precluded the use of this mutant for this study.

Mutation of the four native cysteines to serines did not affect the structural fold of CLIC1. CD spectropolarimetry was used to assess the secondary structural content of oxidized CLIC1$_{24/59}$ in comparison to WT. The CD spectra for both showed a high proportion of α-helical structure with characteristic α-helix minima evident at 208 and 222 nm, and a strong positive ellipticity at 195 nm (Figure 2b). Spectral deconvolution using the CDSSTR analysis program available at DICHROWEB (http://dichroweb.cryst.bbk.ac.uk) (*38*, *39*) showed that both WT and CLIC1$_{24/59}$ contain ~40% α-helical structure, consistent with the crystal structure and suggesting that the mutation of the four native cysteines to serine residues does not affect the fold. CD was also collected in the presence of lipids (1:200 ratio), and no notable change in secondary structure content was observed (data not shown). Tip-dip electrophysiological studies showed that monomeric CLIC1 and the oxidized dimer form produce ion channels in artificial bilayers with similar properties, but mutagenesis of either Cys24 or Cys59 prevents dimer formation and also the ability to form a channel (*6*). Together, these results suggest that, in comparison to WT, the response of the CLIC1$_{24/59}$ construct to oxidative conditions is conserved, and thus, ion channel function is likely maintained.

FRET between Trp35 and Cys89, Cys178, and Cys223. IAEDANS was used to selectively derivatize Cys89, Cys178, or Cys223 of the oxidized dimer form under nonreducing conditions in CLIC1$_{24/59}$(+*Cys89*), CLIC1$_{24/59}$(+*Cys178*), and CLIC1$_{24/59}$(+*Cys223*), respectively. The CLIC1$_{24/59}$ "Cys-less" mutant could not be labeled, confirming that Cys24 and Cys59 are inaccessible to modification because of the formation the Cys24−Cys59 disulfide bond in the oxidized state. The efficiency of labeling of CLIC1 with fluorescent labels for all mutants was greater than 65% (Table 1).

FRET was measured between the Trp35 donor residue and each of the three IAEDANS-modified cysteine residues both in the absence and in the presence of liposomes (Figure 3). The relative decrease in the tryptophan emission peak (~341 nm) of the IAEDANS-labeled samples, compared with WT (unlabeled), coupled with IAEDANS emission, provided clear evidence of energy transfer for all three samples in solution. Significant energy transfer was also observed for each construct upon the immediate addition of lipid vesicles. Twenty-four hours after the addition of lipid vesicles, the degree of energy transfer did not change significantly for CLIC1$_{24/59}$(+*Cys89*) or CLIC1$_{24/59}$(+*Cys178*) (panel a or b, respectively, of Figure 3). However, there was a decrease in the amount of energy transfer upon the addition of lipid for CLIC1$_{24/59}$(+*Cys223*). In the membrane state, minimal energy transfer was noted between Trp35 and Cys223 when compared to the WT (donor only) (Figure 3c). A second probe pair (BDMC−HNB) was thus sought with a longer R_0 to enable more accurate measurement of the Trp35−Cys223 distance in the presence of lipid vesicles (Figure 3d).

The Förster equation was used to calculate the distances between Trp35 and labeled cysteines in both the soluble and

Table 1: FRET Distances Measured between Trp35 and Labeled Cysteines for CLIC in the Soluble Oxidized Dimer and Membrane States and Crystal Structure Distances Obtained from the Oxidized Dimer Crystal Structure (Protein Data Bank entry 1RK4)

					FRET distance		crystal structure distance		
site	probe	labeling ratio	R_0 (Å)	λ_{em} (nm)	R_{sol} (Å) [E_{sol} (%)]	R_{mem} (Å) [E_{mem} (%)]	R_{intra}[a] (Å)	R_{inter}[b] (Å)	$R_{weighted}$[c] (Å)
Trp35 Cys89	intrinsic Trp IAEDANS	0.65 ± 0.12	22	341	24.9 ± 1.4 (38 ± 9)	23.9 ± 1.5 (45 ± 10)	22.2	12.5	12.4
Trp35 Cys178	intrinsic Trp IAEDANS	0.85 ± 0.12	22	341	21.4 ± 1.3 (54 ± 9)	20.8 ± 1.4 (59 ± 9)	12.8	24.5	12.8
Trp35 Cys223	intrinsic Trp IAEDANS	1.06 ± 0.10	22	341	34.1 ± 1.7 (7 ± 4)	44.0 ± 6.7 (0 ± 4)	11.8	33.1	11.8
Cys223 Trp35	BDMC HNB	1.00 ± 0.09 0.65 ± 0.12	38	410	35.7 ± 3.9 (51 ± 9)	48.5 ± 2.6 (13 ± 5)	11.8	33.1	11.8

[a]Intrasubunit distance between CH2 of Trp35 and S of Cys in the same dimer crystal structure subunit. [b]Intersubunit distance between CH2 of Trp35 and S of Cys in opposite dimer crystal structure subunits. [c]Distance values weighted for the expected FRET contribution from both the R_{intra} and R_{inter} Trp35 CH2−Cys S crystal structure distances. Expected efficiencies of energy transfer for a single donor in the presence of two acceptor labels were calculated using the equation $E = R_0^6[R_0^6 + 1/(R_{intra}^{-6} + R_{inter}^{-6})^{-1}]$ (*40*) and corresponding distances determined using the Förster equation (eq 2).

membrane-bound states. The efficiency of energy transfer (E), as determined from the relative decrease in tryptophan emission (341 nm), is given in Table 1 for the soluble state (R_{sol}) and membrane-bound form at 24 h (R_{mem}). The quantum yield (Q_D) and the overlap integral between the Trp35 emission and IAEDANS absorbance [$J(\lambda)$] were determined for CLIC1 in solution to be 0.14 and 4.2×10^{-15} M^{-1} cm^3, respectively. For the BDMC−HNB probe pair, the Q_D was taken to be 0.64 for BDMC (*32*) and $J(\lambda)$ was measured as 2.3×10^{-14} M^{-1} cm^3. From this, R_0 was calculated to be 22 Å for the Trp−IAEDANS interprobe distance pair and 38 Å for the BDMC−HNB pair. Neither value changed in the presence of lipid. Using these R_0 values, the calculated FRET distances are listed in Table 1.

The distance measured from Trp35 to Cys89 in solution and in the presence of lipid vesicles at 24 h did not change significantly (24.9 ± 1.4 and 23.9 ± 1.5 Å, respectively). Likewise, for the Trp35−Cys178 FRET pair, no noticeable change in distance occurred between the two states (21.4 ± 1.3 and 20.8 ± 1.4 Å, respectively). However, a large increase of ≥10 Å between Trp35 and IAEDANS at Cys223 occurred in the presence of lipid vesicles. This increase to 44.0 ± 6.7 Å (E = 0%) represents the upper detection limit for the Trp−IADEANS probe pair. The distance between Trp35 and Cys223 was more accurately determined in the presence of liposomes with the BDMC−HNB probe pair which gave a distance of 48.5 ± 2.6 Å (E = 13%), an increase of 12.8 ± 4.7 Å compared to the distance in the soluble state. There was also good agreement between both probe pairs for the distance obtained for soluble CLIC1 labeled at Cys223 (Trp−IAEDANS, 34.1 ± 1.7 Å; BDMC−HNB, 35.7 ± 3.9 Å).

Approximations for the expected distance between Trp35 and cysteine residues were obtained from the inter-residue distance between the CH2 group of Trp35 and the S group of the labeled cysteine residue in the crystal structure of the oxidized dimer (Table 1). Because of the long effective distance range over which FRET can occur for the probe pairs used in this study, both the intrasubunit (R_{intra}) and intersubunit (R_{inter}) distances contribute to the observed FRET. Symmetry of the dimer molecule (Figure 1) results in a case in which both donor labels are equivalent, and thus, FRET can be considered to occur from a single donor label to two acceptor labels, one in each of the dimer subunits. Therefore, the measured FRET can be analyzed by calculating the contribution from both the intra- and intersubunit crystal structure distances ($R_{weighted}$) (*40*). As expected due to probe length and orientation, the Trp35−IAEDANS distances measured for the three labeled mutants in solution (R_{sol}) are longer than the crystal structure Trp35 CH2−Cys S weighted distances ($R_{weighted}$) measured for the CLIC1 dimer.

Of interest are the changes in the efficiency of energy transfer (E) between Trp35 and cysteine residues measured upon the addition of the liposomes over a 24 h period (Figure 4). Two features of note occurred. Initially, there is a small but noticeable increase in the E for each of the three mutants upon the immediate addition of liposomes. Second, a phase of decreasing E values is then observed over the 24 h time period for each mutant. These changes in E over 24 h are most prominent for $CLIC1_{24/59}$(+*Cys223*). On the basis of previous quantification of membrane insertion over time (*10*) and membrane partitioning observed by EPR, a maximal membrane insertion of ~40% CLIC1 dimer is observed following a 24 h incubation with lipid. Thus, the gradual decrease in the efficiency of energy transfer over the 24 h time period likely represents an increasing population of membrane-inserted CLIC1 as opposed to a single CLIC1 distance increasing in length over time. Thus, for the purpose of modeling the interaction of CLIC1 with the bilayer, the membrane-bound FRET distances [R_{mem} (Table 1)] obtained at the 24 h time point were used. Lipid integrity prevented measurement of time points beyond 24 h.

A Spin-Label at the C-Terminal Cys223 Becomes Mobile upon the Addition of Lipid. The series of EPR spectra of the three MTSSL-labeled CLIC1 mutants in the soluble and membrane-bound form are shown in Figure 5. The membrane-bound state was obtained by spectral subtraction of the corresponding soluble spectra from the composite spectra obtained after direct addition of liposomes. The mobility of the MTSSL spin-label is influenced by its interactions with neighboring side chains and solvent molecules, and thus, changes in spin-label mobility are indicative of changes in its local environment. In the soluble aqueous state, a broad line shape is observed for all three labeled cysteines. Each line shape has two components, one mobile population and a second more immobilized population. This spectral profile is characteristic of a tertiary contact site and is in good agreement with the topological location of all three cysteine in the oxidized dimer crystal structure (Figure 1) (*41*). The spectral component corresponding to the membrane-bound fraction for each labeled mutant was resolved by subtraction of the solution spectrum from the spectrum collected after lipid addition. The partitioning ratio was between 30 and 40% for each mutant, consistent with values obtained for CLIC1 using a

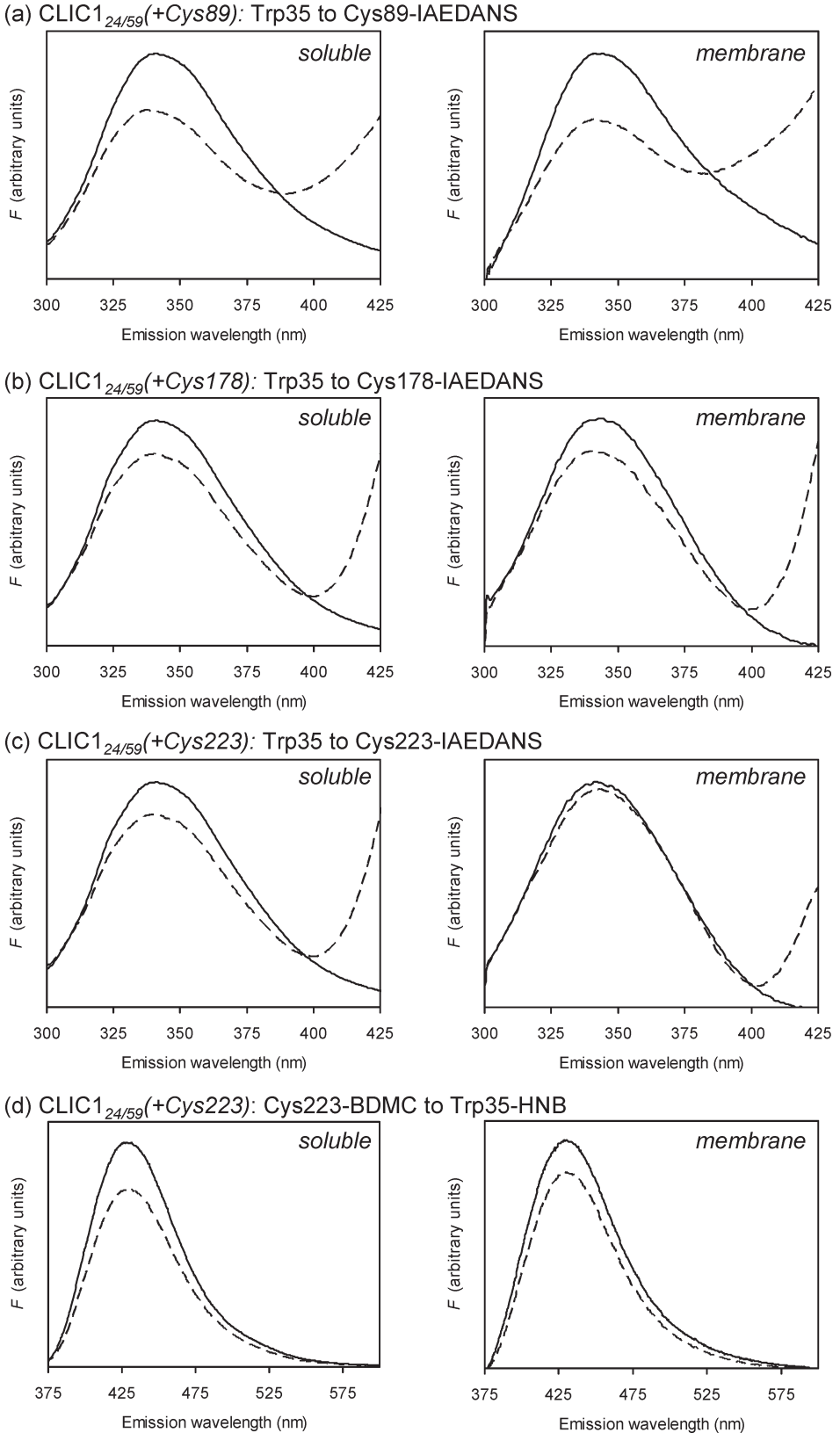

FIGURE 3: FRET between Trp35 and Cys89, Cys178, and Cys223 in the soluble and membrane states. Fluorescence emission spectra of (a) unlabeled CLIC1$_{24/59}$(+*Cys89*) (donor only, solid line) and IAEDANS acceptor-labeled CLIC1$_{24/59}$(+*Cys89*) (donor−acceptor, dashed line), (b) CLIC1$_{24/59}$(+*Cys178*), (c) CLIC1$_{24/59}$(+*Cys223*), and (d) BDMC donor-labeled CLIC1$_{24/59}$(+*Cys223*) (donor only, solid line) and Cys223−BDMC- and Trp35−HNB-labeled CLIC1$_{24/59}$(+*Cys223*) (donor−acceptor, dashed line).

sedimentation assay (*10*). No labeled site displayed motional broadening that would have been indicative of the interaction of the nitroxide label with the more viscous bilayer phase. Instead, the resulting membrane spectrum for the CLIC1$_{24/59}$(+*Cys89*) mutant showed no significant change in mobility, while slight sharpening of the CLIC1$_{24/59}$(+*Cys178*) spectra due to an increase in MTSSL mobility suggests a more solvent-exposed environment for this residue in the membrane-bound form. More

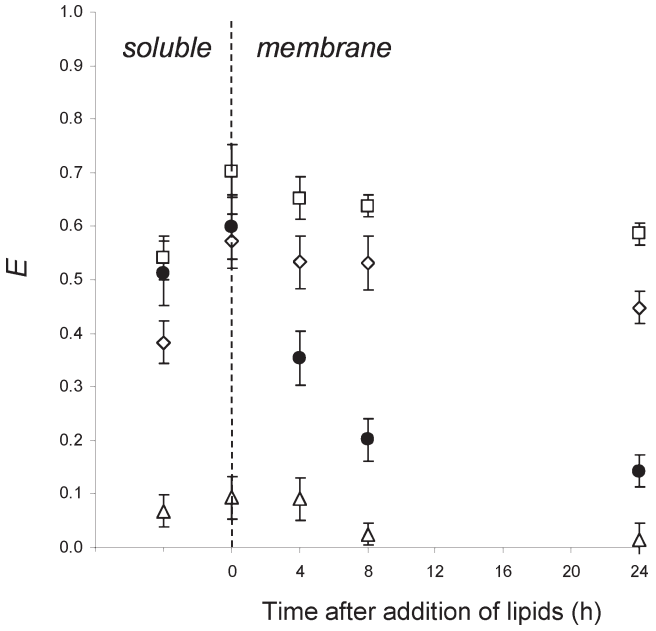

FIGURE 4: Efficiency of energy transfer (E) from Trp35 to cysteine FRET in the soluble state, initially upon addition of lipid over a 24 h time course: Trp35−Cys89-IAEDANS (◇), Trp35−Cys178-IAEDANS (□), Trp35−Cys223-IAEDANS (△), and Cys223-BDMC−Trp35-HNB (●).

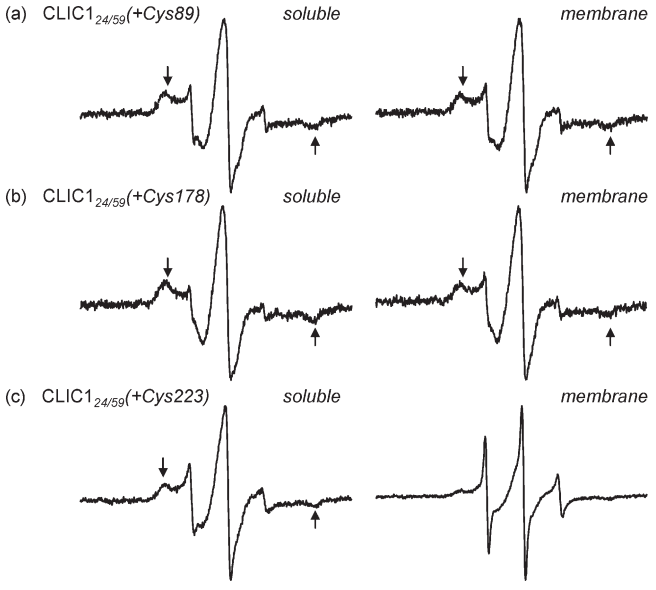

FIGURE 5: First-derivative EPR spectra of CLIC1 mutants labeled with MTSSL (left) in aqueous solution (soluble) and (right) bound to LUVs at a molar ratio of 500:1 (membrane), obtained by spectral subtraction. Scan widths are 120 G, and spectra are normalized to the amplitude of the center peak. The black arrows mark the location of the outer hyperfine extrema and indicate a second immobilized component. The sharpening of the EPR spectra and the loss of the second immobile component for CLIC1$_{24/59}$(+*Cys223*) in the membrane state reflect a significant increase in the level of motional averaging of the C-domain region upon membrane interaction.

notably, CLIC1$_{24/59}$(+*Cys223*) exhibited a dramatic change in the EPR line shape upon addition of lipid. The CLIC1$_{24/59}$(+*Cys223*) membrane-bound spectrum resembles the three-sharp line hyperfine pattern indicative of a highly mobile spin-label sitting in a completely solvent-exposed environment. The loss of steric constraint for this residue is suggestive of an unrestricted

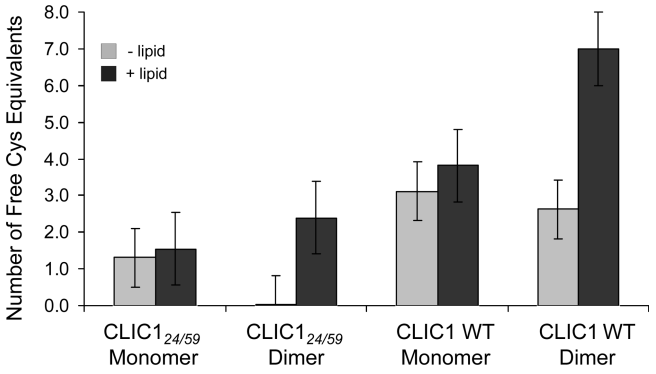

FIGURE 6: Ellman's reagent assay for the measurement of free cysteine equivalents. Free sulfhydryl groups in the CLIC1$_{24/59}$ and CLIC1 WT monomer and dimer were quantified, both in the soluble state (−lipid) and in the presence of lipids (+lipid). The equivalent numbers of free cysteines per CLIC molecule are shown (n = 3).

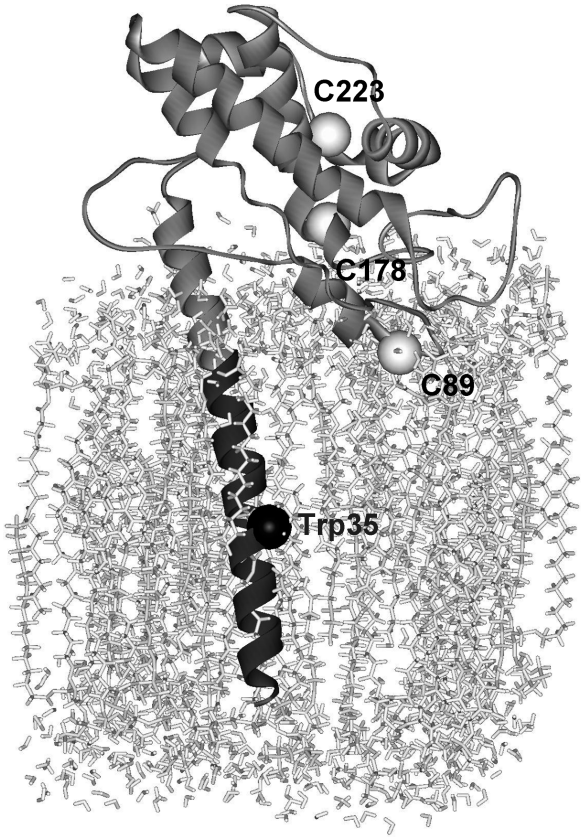

FIGURE 7: Model of the CLIC1 membrane state showing the separation of the N- and C-domains as CLIC1 traverses the membrane. The distances between Trp35 (black sphere), located within the N-terminal PTM (black), and Cys89, Cys178, and Cys223 (gray spheres), located in the C-domain, are consistent with the observed membrane-state FRET distances.

region or possibly a largely unstructured region for the C-terminus in the membrane-bound state.

Breakage of the Cys24−Cys59 Bond in the Presence of Lipids. No significant change in the proportion of free sulfhydryl groups for the CLIC1$_{24/59}$ monomer occurs upon the addition of lipid (Figure 6). However, for the CLIC1$_{24/59}$ dimer, a significant increase from approximately zero free sulfhydryl groups in solution to approximately two free sulfhydryl equivalents is observed upon addition of lipids. As CLIC1$_{24/59}$ contains only two cysteines (Cys24 and Cys59), this increase in free sulfhydryl

content likely corresponds to dissociation of the Cys24−Cys59 disulfide. A similar increase in free sulfhydryl content is also seen for the CLIC1 WT dimer in the presence of lipids, suggesting all cysteines in the membrane state are now accessible.

Modeling of a CLIC1 Integral Membrane Form. To interpret our observations in terms of structural changes associated with the interaction of CLIC1 with the bilayer, we modeled the membrane state of CLIC1 using the observed 24 h membrane FRET distances obtained as constraints between domains flanking the PTM spanning segment. FRET distances were treated as distances between the CH2 atom of the Trp35 aromatic ring and the S group of the cysteine residue. As labels are not explicitly modeled, we applied an error of ±4 Å to account for label orientation. Rigid body minimization was applied to the soluble oxidized CLIC1 half-dimer structure where the disulfide bond between Cys24 and Cys59 was reduced, as suggested by the exposure of these residues to Ellman's reagent in the presence of lipid, and the PTM was allowed to rearrange into an extended conformation to span the bilayer and the three domains composed of residues 22−58, 79−90, and 111−234 treated as rigid bodies. Our resulting model when embedded in a lipid bilayer shows the CLIC1 N-terminal domain (residues 22−58) crossing the bilayer and the C-terminal domain (residues 111−234) separating from the N-terminal domain and residing on the membrane surface (Figure 7). The distances between the CH2 group of Trp35 and the S group of cysteine residues 89, 178, and 223 in the final model are 18, 27, and 42 Å, respectively. These are all in good agreement (< 6 Å) with the R_{mem} FRET distances (Table 1) when the method of measurement, probe size, and probe flexibility are taken into consideration. Our model is consistent with the current hypothesis that the N- and C-termini of CLIC1 reside on opposite sides of the bilayer and that the N-terminal PTM is buried within the bilayer.

DISCUSSION

Despite extensive structural studies of the soluble forms of several CLIC family members, the structure of the membrane-bound state is still unknown. This is largely due to the metamorphic nature of the CLIC protein family which has made them particularly difficult targets to study using standard techniques, including crystallography and NMR. Both these techniques are often thwarted when multiple protein conformations are present. On the other hand, FRET and EPR can allow us to examine an ensemble of protein conformations under physiologically relevant conditions. However, interpretation of this data is dependent on whether an estimation of the population of different protein conformation is available. There are at least three possible states for CLIC1, a monomeric soluble form, an oxidized soluble dimer form, and a membrane state. Current evidence suggests a CLIC1 membrane structure in which the N- and C-termini are on opposite sides of the bilayer with N-terminal residues 24−46 forming the putative transmembrane region. The transition between the soluble CLIC forms and such a membrane-inserted conformation must involve large-scale rearrangement to allow the CLIC module to traverse the lipid bilayer and confer favorable interactions with the membrane. However, evidence of such a dramatic structural change upon interaction of the CLIC protein with the membrane has been lacking. The most notable result from our FRET and EPR experiments, described herein, is confirmation that a structural change indeed occurs within CLIC1 upon membrane interaction. Modeling of the steady-state FRET shows that the change in distances upon membrane interaction can be successfully integrated into a low-resolution membrane model whereby separation of the N- and C-domains of CLIC1 occurs as the PTM spans the bilayer. Alternatively, the data may also be interpreted simply by local disordering of the CLIC1 C-terminus.

One significant advantage of using FRET and EPR to probe changes in protein structure is that natural amino acids can be utilized as intrinsic fluorescence labels (Trp) or targeted for the attachment of extrinsic fluorescent or EPR probes (Cys). CLIC1 contains a single tryptophan residue (Trp35 within the PTM) but is cysteine rich, and thus, the development of a viable strategy for obtaining site-specific labeling of the cysteines was required. Of the six native CLIC1 cysteines, three are highly conserved (Cys24, Cys178, and Cys223). Cys24 is an essential residue that is conserved in the mammalian CLICs. Cys24 is necessary for optimal CLIC1 ion channel activity (*6*) and is also the site for redox regulation (*6*, *7*, *10*). More recently, the importance of this redox sensitive residue was further highlighted in CLIC4 where it was shown to serve as an active site residue required in the translocation of CLIC4 to the plasma membrane (*42*). Thus, preserving Cys24 in our labeling constructs and the subsequent protection of Cys24 during the labeling procedure were essential. Our labeling strategy therefore involved the isolation of the oxidized noncovalent CLIC1 dimer in which Cys24 and Cys59 are protected from further chemical modification in solution by formation of the Cys24−Cys59 disulfide. This Cys24−Cys59 covalent linkage remained intact during the targeted labeling of the other individual native cysteines. The two other conserved native mammalian CLIC cysteine residues (Cys178 and Cys223 of CLIC1) do not appear to be necessary for translocation of CLIC4 to the membrane (*42*) and thus may not be essential for CLIC membrane insertion.

The fortuitous redox response of CLIC1 enabled us to successfully collect structural data in both the presence and absence of membranes while preserving the integrity of the construct. It is important to note that the distances measured by FRET correspond to distances between donor and acceptor label molecules and thus will deviate from the CLIC1 crystallographic distances. Upon comparison of our FRET interlabel distances to the crystal structure distances, an error of approximately 8−10 Å serves as an appropriate estimate of the discrepancies that arise from experimental uncertainties and the size and location of the FRET labels (*43*). Additionally, it is also necessary to consider that the FRET contributions in solution arise from an ensemble of both the distance between the donor and acceptor label in the same dimer subunit (R_{intra}) and the donor and acceptor label in the opposite dimer subunit (R_{inter}). Because of the nature of the FRET technique, shorter distances contribute more to the efficiency of energy transfer measured, and thus, the FRET distances measured are biased toward the nearest-neighbor acceptor. Thus, for example, for FRET between Trp35 and Cys178 or Cys223, the shorter R_{intra} distance dominates, while a similar contribution from both the R_{intra} and R_{inter} Trp35−Cys89 distance exists (Table 1).

Considering the information given above, the Trp35−Cys89 and −Cys178 FRET distances were in good agreement with those predicted from the crystal structure. The greatest difference was noted for the Trp35−Cys223 distance, most likely because of the proximity of Cys223 to the C-terminus, which is not surprising because of the location of this residue on a loop preceding the last helix observed in the dimer crystal structure (h9). Using the

FRET technique, it is our relative distance changes that can be more accurately measured than the absolute distances. As an added precaution, we also employed the use of two FRET labeling pairs in which the direction of the energy transfer process is reversed. This gave us good consistency upon measurement of the Trp35−Cys223 distance in solution. Clearly, when distance changes are being determined, the error is also minimized by the selective placement of the labels for distances similar to the R_0 for the chosen probe pair. Using the Trp35−IAEDANS FRET pair, the distance from Trp35 to Cys223 shows a measurable increase of ~10 Å upon conversion to the membrane-bound state, however, the increase bringing us to the upper limit of detection for this probe pair (44 Å). The distance between Trp35 and Cys223 in the membrane state was also performed with the BDMC−HNB FRET pair with a longer R_0 of 38 Å, providing a distance in the presence of membranes of 48.5 Å, an increase of ~13 Å from the distance measured in solution. The notable change in mobility detected for the nitroxide spin-label attached to Cys223 confirms that the conformational change detected by the Trp35−Cys223 FRET measurement modulates tertiary interactions within CLIC1.

How can the data collected in the presence of the membrane be interpreted? Our FRET distances between Trp35 in the N-domain PTM and cysteine residues throughout the C-domain portion of CLIC1 clearly detected a structural change occurs upon interaction with the lipid bilayer. The data can be interpreted in two ways. The most direct interpretation is simply the local unraveling of the C-terminal region to an extended and unstructured state upon lipid binding. Cys223 is in the loop between short helix 8 (residues 218−222) and helix 9 (residues 226−233) in the dimer crystal structure. The simplest assumption is that unraveling of helix 8, and possibly helix 9, from coil to random coil, can account for the increase observed in the FRET distance. The location of the spin-label at Cys223 would also be sensitive to such a structural transition occurring for adjoining helices, which was indeed observed. Our alternative model (Figure 7) has CLIC1 as an integral membrane protein. This model is based on previous findings that the CLIC1 dimer is capable of undergoing membrane insertion to form ion channels similar to those observed in vivo (*6*). It is also now well believed that the highly conserved 60-residue N-terminal CLIC PTM is likely to be the motif required for translocation of the CLIC proteins from solution into the transmembrane form (*10*, *29*, *30*, *44*). If this view is correct, then upon membrane insertion, the separation of the two CLIC domains must occur for the N-domain of CLIC1 to penetrate across the bilayer, most likely forming a single PTM helix. Our rigid body model of the integral membrane state using the FRET distance constraints is qualitatively consistent with the movement of the N-domain of CLIC1 away from the C-domain with the insertion of the N-terminal domain across the bilayer. Such a model incorporates the large conformational metamorphosis expected to occur to expose buried hydrophobic residues within CLIC1 to allow the replacement of protein−protein interactions with protein−lipid interactions. Recent results from amide hydrogen−deuterium exchange mass spectrometry of CLIC1, albeit performed in the absence of membrane, indicate that the N-domain, encompassing the PTM domain, becomes destabilized at low pH while the structure of the all-helical C-domain remains intact (*28*). It is suggested that encountering such an acidic environment prior to membrane insertion primes the solution structure of CLIC1 by lowering the activation energy barrier for conversion to the membrane-inserted form via the N-domain inserting into the bilayer. Our spectral changes noted in the presence of the membrane extend further upon this insertion model by confirming that a conformational change does indeed occur which can be ascribed to the simple movement of the N-domain away from the C-domain.

Our model of the integral membrane state of CLIC1 now requires future experimental validation and refinement. While the conformation of the PTM region in the membrane-inserted CLIC1 form is still unknown, it is most likely to be helical with h1 (residues 24−42) forming the majority of the PTM region. Residues 42−46 also exhibit a propensity to form a helix with potential N- and C-capping motifs (*28*) and are highly dynamic as seen in the rearranged structure of the oxidized dimeric form (*6*). Thus, for the purpose of modeling, the PTM was forced into a single transmembrane helix. However, for this region to function as a single-pass transmembrane domain, it must become separated from the C-domain about a hinge region or regions. An alignment between both the unstructured loop regions of the CLIC1 crystal structure and the main regions of the N-domain identified by Stoychev et al. undergoing pH-induced plasticity yields two potential hinge regions within CLIC1. These potential hinges are between residues 58 and 79 and residues 90 and 111. In our model, these regions were allowed to hinge around the linker between the N- and C-domains while the remaining portions of CLIC1 (residues 22−58, 79−90, and 111−234) were rotated as rigid bodies within the constraints of the observed FRET changes. However, as already discussed, we cannot distinguish whether the spectral changes we note at region Cys223 are truly representative of whole domain movement or the result of local C-terminal unravelling within the vicinity of the labeling site. Probing into the secondary elements on either side of Cys223 is needed to determine if the secondary structure of either helix 8 or 9 remains in the membrane state. Additional probing between other secondary structural elements of the C-domain and the N-domain will also confirm the modeled hinge regions within the CLIC1 molecule.

It is important to note that the steady-state FRET measurements, on which our model was developed, do not take into account any additional CLIC1 membrane conformations that may be present beyond a single transmembrane state. Further estimates of the CLIC1 metamorphosis response to membrane can be obtained on the basis of how much CLIC1 is expected to insert into the membrane. The simplest case is that in which only two states are present, soluble and membrane-inserted. This is unlikely to be true, and it is not unreasonable to assume that there are other intermediate states that we are detecting that may include membrane docking or priming states or also higher oligomeric state(s). On the basis of a 40% partitioning value for the CLIC1 dimer incubated with the membrane (*10*), an upper limit of ~54 Å may be calculated for the Trp35−Cys223 distance. This value is 8 Å longer than what we can detect on our bulk sample but still consistent with our model for the movement of the N-domain away from the C-domain.

An interesting effect observed in our FRET results is an initial small (up to ~10%) but consistent increase in the efficiency of energy transfer between Trp35 and each of the three cysteines upon immediate mixing with liposomes (Figure 4). Such an effect may arise from either the shortening of an existing distance or interaction with additional close range acceptors. It is tempting to suggest that this result is suggestive of the existence of an initial membrane docking or associating form that is different from the membrane-inserted form, which has previously been

proposed (*6*, *10*, *28*). Further investigation is required to clarify the nature of any CLIC1 membrane insertion intermediates and whether these involve dissociation of the dimer or formation of other oligomeric species.

One remaining puzzle regarding ion channel formation by the oxidized dimer in lipid bilayers is the fate of the disulfide bond between Cys24 and Cys59. Intuitively, if CLIC family members follow an evolutionarily conserved membrane insertion mechanism, it is unlikely disulfide formation is involved as the Cys59 residue is not conserved in other CLICs. Furthermore, if the PTM domain (residues 24−46) is to span the membrane, then this disulfide bond must be reduced. The observed increase in free sulfhydryl groups upon addition of lipid to CLIC1 dimer in solution (Figure 6) suggests the Cys24−Cys59 disulfide dissociates in the presence of the lipid bilayer. In WT oxidized CLIC1, one can postulate that an isomerization between free cysteine and the Cys24−Cys59 disulfide bond releases the PTM or that the lecithin membranes contain soybean molecules that can reduce this disulfide bond. However, the mechanism of disulfide bond disruption is unknown. In this paper, use of disulfide formation in the CLIC1 oxidized dimer has proven to be advantageous in designing a novel strategy for obtaining site-specific labeling of single cysteines by allowing selective protection of the functionally conserved Cys24 that would otherwise have proven to be exceedingly difficult. Even if the dimer is not formed in vivo, the process of dimer formation does not preclude membrane insertion (*6*, *10*). Hence, disruption of the Cys24−Cys59 bond is implicit in our model.

In summary, the structural change detected within CLIC1 upon membrane interaction reinforces the dynamic nature of the CLIC proteins. Members of the CLIC family appear to be capable of displaying several structural conformations, which may be required for performing their many putative functional cellular roles. At present and in the absence of a CLIC crystal structure of the integral membrane form, FRET and EPR have, and will continue to be, extremely useful tools for addressing a large number of previously inaccessible questions. Ongoing work to further probe the integral membrane form will allow us to refine the integral membrane state and answer questions such as the structural nature of the PTM within the bilayer and clarify the location of the hinge regions. Once these important structural features are established within the membrane state, only then can future work clearly explore varying environmental triggers controlling binding, insertion, and oligomeric formation processes, such as lipid composition, pH, and oxidation.

REFERENCES

1. Murzin, A. G. (2008) Biochemistry. Metamorphic proteins. *Science 320*, 1725–1726.
2. Harrop, S. J., DeMaere, M. Z., Fairlie, W. D., Reztsova, T., Valenzuela, S. M., Mazzanti, M., Tonini, R., Qiu, M. R., Jankova, L., Warton, K., Bauskin, A. R., Wu, W. M., Pankhurst, S., Campbell, T. J., Breit, S. N., and Curmi, P. M. (2001) Crystal structure of a soluble form of the intracellular chloride ion channel CLIC1 (NCC27) at 1.4-Å resolution. *J. Biol. Chem. 276*, 44993–45000.
3. Tulk, B. M., Kapadia, S., and Edwards, J. C. (2002) CLIC1 inserts from the aqueous phase into phospholipid membranes, where it functions as an anion channel. *Am. J. Physiol. 282*, C1103–C1112.
4. Warton, K., Tonini, R., Fairlie, W. D., Matthews, J. M., Valenzuela, S. M., Qiu, M. R., Wu, W. M., Pankhurst, S., Bauskin, A. R., Harrop, S. J., Campbell, T. J., Curmi, P. M., Breit, S. N., and Mazzanti, M. (2002) Recombinant CLIC1 (NCC27) assembles in lipid bilayers via a pH-dependent two-state process to form chloride ion channels with identical characteristics to those observed in Chinese hamster ovary cells expressing CLIC1. *J. Biol. Chem. 277*, 26003–26011.
5. Berryman, M., Bruno, J., Price, J., and Edwards, J. C. (2004) CLIC-5A functions as a chloride channel in vitro and associates with the cortical actin cytoskeleton in vitro and in vivo. *J. Biol. Chem. 279*, 34794–34801.
6. Littler, D. R., Harrop, S. J., Fairlie, W. D., Brown, L. J., Pankhurst, G. J., Pankhurst, S., DeMaere, M. Z., Campbell, T. J., Bauskin, A. R., Tonini, R., Mazzanti, M., Breit, S. N., and Curmi, P. M. (2004) The intracellular chloride ion channel protein CLIC1 undergoes a redox-controlled structural transition. *J. Biol. Chem. 279*, 9298–9305.
7. Singh, H., and Ashley, R. H. (2006) Redox regulation of CLIC1 by cysteine residues associated with the putative channel pore. *Biophys. J. 90*, 1628–1638.
8. Cromer, B. A., Gorman, M. A., Hansen, G., Adams, J. J., Coggan, M., Littler, D. R., Brown, L. J., Mazzanti, M., Breit, S. N., Curmi, P. M., Dulhunty, A. F., Board, P. G., and Parker, M. W. (2007) Structure of the Janus protein human CLIC2. *J. Mol. Biol. 374*, 719–731.
9. Singh, H., and Ashley, R. H. (2007) CLIC4 (p64H1) and its putative transmembrane domain form poorly selective, redox-regulated ion channels. *Mol. Membr. Biol. 24*, 41–52.
10. Goodchild, S. C., Howell, M. W., Cordina, N. M., Littler, D. R., Breit, S. N., Curmi, P. M., and Brown, L. J. (2009) Oxidation promotes insertion of the CLIC1 chloride intracellular channel into the membrane. *Eur. Biophys. J. 39*, 129–138.
11. Morris, M. J., Craig, S. J., Sutherland, T. M., Board, P. G., and Casarotto, M. G. (2009) Transport of glutathione transferase-fold structured proteins into living cells. *Biochim. Biophys. Acta 1788*, 676–685.
12. Valenzuela, S. M., Martin, D. K., Por, S. B., Robbins, J. M., Warton, K., Bootcov, M. R., Schofield, P. R., Campbell, T. J., and Breit, S. N. (1997) Molecular cloning and expression of a chloride ion channel of cell nuclei. *J. Biol. Chem. 272*, 12575–12582.
13. Berry, K. L., Bulow, H. E., Hall, D. H., and Hobert, O. (2003) A *C. elegans* CLIC-like protein required for intracellular tube formation and maintenance. *Science 302*, 2134–2137.
14. Littler, D. R., Harrop, S. J., Brown, L. J., Pankhurst, G. J., Mynott, A. V., Luciani, P., Mandyam, R. A., Mazzanti, M., Tanda, S., Berryman, M. A., Breit, S. N., and Curmi, P. M. (2007) Comparison of vertebrate and invertebrate CLIC proteins: The crystal structures of *Caenorhabditis elegans* EXC-4 and *Drosophila melanogaster* DmCLIC. *Proteins 71*, 364–378.
15. Elter, A., Hartel, A., Sieben, C., Hertel, B., Fischer-Schliebs, E., Luttge, U., Moroni, A., and Thiel, G. (2007) A plant homolog of animal chloride intracellular channels (CLICs) generates an ion conductance in heterologous systems. *J. Biol. Chem. 282*, 8786–8792.
16. Littler, D. R., Harrop, S. J., Goodchild, S. C., Phang, J. M., Mynott, A. V., Jiang, L., Valenzuela, S. M., Mazzanti, M., Brown, L. J., Breit, S. N., and Curmi, P. M. G. (2010) The enigma of the CLIC proteins: Ion channels, redox proteins, enzymes, scaffolding proteins? *FEBS Lett. 584*, 2093–2101.
17. Valenzuela, S. M., Mazzanti, M., Tonini, R., Qiu, M. R., Warton, K., Musgrove, E. A., Campbell, T. J., and Breit, S. N. (2000) The nuclear chloride ion channel NCC27 is involved in regulation of the cell cycle. *J. Physiol. 529* (Part 3), 541–552.
18. Berryman, M. A., and Goldenring, J. R. (2003) CLIC4 is enriched at cell-cell junctions and colocalizes with AKAP350 at the centrosome and midbody of cultured mammalian cells. *Cell Motil. Cytoskeleton 56*, 159–172.
19. Fernandez-Salas, E., Suh, K. S., Speransky, V. V., Bowers, W. L., Levy, J. M., Adams, T., Pathak, K. R., Edwards, L. E., Hayes, D. D., Cheng, C., Steven, A. C., Weinberg, W. C., and Yuspa, S. H. (2002) mtCLIC/CLIC4, an organellular chloride channel protein, is increased by DNA damage and participates in the apoptotic response to p53. *Mol. Cell. Biol. 22*, 3610–3620.
20. Suh, K. S., Mutoh, M., Gerdes, M., Crutchley, J. M., Mutoh, T., Edwards, L. E., Dumont, R. A., Sodha, P., Cheng, C., Glick, A., and Yuspa, S. H. (2005) Antisense suppression of the chloride intracellular channel family induces apoptosis, enhances tumor necrosis factor α-induced apoptosis, and inhibits tumor growth. *Cancer Res. 65*, 562–571.
21. Shiio, Y., Suh, K. S., Lee, H., Yuspa, S. H., Eisenman, R. N., and Aebersold, R. (2006) Quantitative proteomic analysis of myc-induced apoptosis: A direct role for Myc induction of the mitochondrial chloride ion channel, mtCLIC/CLIC4. *J. Biol. Chem. 281*, 2750–2756.
22. Edwards, J. C., Cohen, C., Xu, W., and Schlesinger, P. H. (2006) c-Src control of chloride channel support for osteoclast HCl transport and bone resorption. *J. Biol. Chem. 281*, 28011–28022.
23. Bohman, S., Matsumoto, T., Suh, K., Dimberg, A., Jakobsson, L., Yuspa, S., and Claesson-Welsh, L. (2005) Proteomic Analysis of

Vascular Endothelial Growth Factor-induced Endothelial Cell Differentiation Reveals a Role for Chloride Intracellular Channel 4 (CLIC4) in Tubular Morphogenesis. *J. Biol. Chem. 280*, 42397–42404.
24. Chalothorn, D., Zhang, H., Smith, J. E., Edwards, J. C., and Faber, J. E. (2009) Chloride intracellular channel-4 is a determinant of native collateral formation in skeletal muscle and brain. *Circ. Res. 105*, 89–98.
25. Tung, J. J., Hobert, O., Berryman, M., and Kitajewski, J. (2009) Chloride intracellular channel 4 is involved in endothelial proliferation and morphogenesis in vitro. *Angiogenesis 12*, 209–220.
26. Ulmasov, B., Bruno, J., Gordon, N., Hartnett, M. E., and Edwards, J. C. (2009) Chloride intracellular channel protein-4 functions in angiogenesis by supporting acidification of vacuoles along the intracellular tubulogenic pathway. *Am. J. Pathol. 174*, 1084–1096.
27. Fanucchi, S., Adamson, R. J., and Dirr, H. W. (2009) Formation of an Unfolding Intermediate State of Soluble Chloride Intracellular Channel Protein CLIC1 at Acidic pH. *Biochemistry 48*, 11674–11681.
28. Stoychev, S. H., Nathaniel, C., Fanucchi, S., Brock, M., Li, S., Asmus, K., Woods, V. L., Jr., and Dirr, H. W. (2009) Structural dynamics of soluble chloride intracellular channel protein CLIC1 examined by amide hydrogen-deuterium exchange mass spectrometry. *Biochemistry 48*, 8413–8421.
29. Tonini, R., Ferroni, A., Valenzuela, S. M., Warton, K., Campbell, T. J., Breit, S. N., and Mazzanti, M. (2000) Functional characterization of the NCC27 nuclear protein in stable transfected CHO-K1 cells. *FASEB J. 14*, 1171–1178.
30. Duncan, R. R., Westwood, P. K., Boyd, A., and Ashley, R. H. (1997) Rat brain p64H1, expression of a new member of the p64 chloride channel protein family in endoplasmic reticulum. *J. Biol. Chem. 272*, 23880–23886.
31. Hudson, E. N., and Weber, G. (1973) Synthesis and characterization of two fluorescent sulfhydryl reagents. *Biochemistry 12*, 4154–4161.
32. Farinotti, R., Siard, Ph., Bourson, J., Kirkiacharian, S., Valeur, B., and Mahuzier, G. (1983) 4-Bromomethyl-6,7-dimethoxycoumarin as a fluorescent label for carboxylic acids in chromatographic detection. *J. Chromatogr., A 269*, 81–95.
33. Barman, T. E., and Koshland, D. E. J. (1967) A colorimetric procedure for the quantitative determination of tryptophan residues in proteins. *J. Biol. Chem. 242*, 5771–5776.
34. Wang, C. K., and Cheung, H. C. (1986) Proximity relationship in the binary complex formed between troponin I and troponin C. *J. Mol. Biol. 191*, 509–521.
35. Melhuish, W. H. (1961) Quantum efficiencies of fluorescence of organic substances: Effect of solvent and concentration of fluorescent solute. *J. Phys. Chem. 65*, 229–235.
36. Brunger, A. T. (2007) Version 1.2 of the Crystallography and NMR system. *Nat. Protoc. 2*, 2728–2733.
37. Brunger, A. T., Adams, P. D., Clore, G. M., DeLano, W. L., Gros, P., Grosse-Kunstleve, R. W., Jiang, J. S., Kuszewski, J., Nilges, M., Pannu, N. S., Read, R. J., Rice, L. M., Simonson, T., and Warren, G. L. (1998) Crystallography & NMR system: A new software suite for macromolecular structure determination. *Acta Crystallogr. D54*, 905–921.
38. Lobley, A., Whitmore, L., and Wallace, B. A. (2002) DICHROWEB: An interactive website for the analysis of protein secondary structure from circular dichroism spectra. *Bioinformatics 18*, 211–212.
39. Sreerama, N., and Woody, R. W. (2000) Estimation of protein secondary structure from circular dichroism spectra: Comparison of CONTIN, SELCON, and CDSSTR methods with an expanded reference set. *Anal. Biochem. 287*, 252–260.
40. Moens, P. D., Wahl, M. C., and Jameson, D. M. (2005) Oligomeric state and mode of self-association of *Thermotoga maritima* ribosomal stalk protein L12 in solution. *Biochemistry 44*, 3298–3305.
41. McHaourab, H. S., Lietzow, M. A., Hideg, K., and Hubbell, W. L. (1996) Motion of spin-labeled side chains in T4 lysozyme. Correlation with protein structure and dynamics. *Biochemistry 35*, 7692–7704.
42. Ponsioen, B., van Zeijl, L., Langeslag, M., Berryman, M., Littler, D., Jalink, K., and Moolenaar, W. H. (2009) Spatiotemporal regulation of chloride intracellular channel protein CLIC4 by RhoA. *Mol. Biol. Cell 20*, 4664–4672.
43. Majumdar, Z. K., Hickerson, R., Noller, H. F., and Clegg, R. M. (2005) Measurements of internal distance changes of the 30S ribosome using FRET with multiple donor-acceptor pairs: Quantitative spectroscopic methods. *J. Mol. Biol. 351*, 1123–1145.
44. Berry, K. L., and Hobert, O. (2006) Mapping functional domains of chloride intracellular channel (CLIC) proteins in vivo. *J. Mol. Biol. 359*, 1316–1333.